

## Dependence of band structure and exciton properties of encapsulated WSe<sub>2</sub> monolayers on the hBN-layer thickness

Iann C. Gerber\* and Xavier Marie

*LPCNO, Université Fédérale de Toulouse Midi-Pyrénées, INSA-CNRS-UPS, 135 Avenue de Rangueil, 31077 Toulouse, France*

(Received 5 October 2018; published 19 December 2018)

The optical properties of two-dimensional transition-metal dichalcogenide monolayers, such as MoS<sub>2</sub> or WSe<sub>2</sub> are dominated by excitons, Coulomb bound electron-hole pairs. Screening effects due to the presence of hexagonal-boron nitride (hBN) surrounding layers have been investigated by solving the Bethe-Salpeter equation on top of *GW* wave functions in density functional theory calculations. We have calculated the dependence of both the quasiparticle gap and the binding energy of the neutral exciton ground-state  $E_b$  as a function of the hBN-layer thickness. This paper demonstrates that the effects of screening at this level of theory are more short ranged than is widely believed. The encapsulation of a WSe<sub>2</sub> monolayer by three sheets of hBN ( $\sim 1$  nm) already yields a 20% decrease in  $E_b$ , whereas the maximal reduction is 27% for thick hBN. We have performed similar calculations in the case of a WSe<sub>2</sub> monolayer deposited on stacked hBN layers. These results are compared to the recently proposed quantum electrostatic heterostructure approach.

DOI: [10.1103/PhysRevB.98.245126](https://doi.org/10.1103/PhysRevB.98.245126)

### INTRODUCTION

Monolayers (MLs) of transition-metal dichalcogenides (TMDCs), based on Mo or W metals, have been the subject of intense research thanks to a fascinating combination of properties [1]. Indeed, TMDC monolayers exhibit a direct fundamental band gap in the optical range [2,3] contrary to graphene, which makes them good materials for a new generation of optoelectronic devices [4]. Interestingly, the electronic and optical properties of these systems are dominated by robust excitons, i.e., Coulomb bound electron-hole pairs [5–8]. Their very high binding energies of a few hundred meV are due to a reduced Coulomb screening in combination with a strong two-dimensional (2D) quantum confinement and a large effective mass. Owing to the extreme confinement in the perpendicular direction to the TMDC plane, excitons are particularly sensitive to the local environment surrounding the monolayer either because of the presence of a substrate or because of even more complex stacking configurations [9–16]. In general, the band structures of the constituent 2D crystals and band alignment across the interfaces of a van der Waals heterostructure (vdWH) depend on many factors: interlayer hybridization, charge transfer, dielectric screening, proximity-induced spin-orbit interactions, etc. However, in many vdWHs based on TMDCs, the weak interlayer binding suggests that each vdWH individual layer mainly keeps its original 2D properties modified only by the long-range Coulomb interaction with their immediate neighboring layers. From an experimental point of view, one usually observes a rather weak dependence of the exciton ground-state absolute energy by varying the dielectric environment since both the quasiparticle (QP) gap (also called the free-carrier gap,

noted  $E_g$  below) and the exciton binding energy vary and the corresponding changes almost compensate each other. However, recent measurements of the diamagnetic shift of the exciton transition in high magnetic fields evidenced clearly the change in exciton size and binding energy by encapsulating WSe<sub>2</sub> monolayers with hBN [17,18]. A significant reduction of the exciton binding energy has also been observed by encapsulation of TMDC monolayers with graphene layers [19]. Using metals, such as Au as a substrate, has been also reported, showing a large reduction of the neutral exciton binding energy [13].

The dependence of the TMDC monolayer band structure and exciton binding energy as a function of the substrate thickness has been less studied [19–21]. The key fundamental question is: What is the typical range for the dielectric environment influence? The variation of the exciton energy of a WS<sub>2</sub> monolayer as a function of the number of layers of capping graphene was measured [19]; the impact of a single layer of graphene was clearly evidenced. The encapsulation with hBN, a material with a weaker dielectric constant compared to graphene, presents major advantages as it yields very narrow homogeneously broadened exciton lines which allow, for instance, the realization of atomically thin mirrors [22–27]. In comparison with a WSe<sub>2</sub> ML deposited on a SiO<sub>2</sub> substrate, redshifts of the neutral exciton energy in the range of 15–30 meV were observed when the ML was transferred on a hBN-thick-layer substrate or encapsulated by hBN [10,19,22].

On a theoretical level, the effect of an anisotropic dielectric environment on the excitonic properties of an atomically thin layer is a complex issue with nonanalytic solutions. A first approach is to use an approximate form for the radial dependence of the Coulomb potential in the framework of the Wannier-Mott Hamiltonian for thin films [18,28–31]. More recently, several models have been proposed to study the

\*igerber@insa-toulouse.fr

evolution of the quasiparticle (QP) band gaps and the excitonic properties from the ML to the bulk limit [32,33]; other studies investigate the effects of the substrate dielectric environment [32–37] or more complex heterostructures [12,38–40]. Among these approaches, the quantum electrostatic heterostructure (QEH) model is probably the most popular to study complex vdWHs [41] due to its versatility and simplicity [42].

Very few *ab initio* studies at the density functional theory (DFT) level and beyond can be found in the literature. Indeed, the incommensurate nature of vdWHs presents a great challenge for first-principles calculations because it is generally not possible to represent the heterostructure in a computational cell that is small enough to allow the calculation to be performed without straining one or more of the layers and thereby alter its electronic properties. The problem is particularly severe for many-body calculations for which the computational cost grows rapidly with system size. However, for some specific and well-defined configurations [43], *GW* coupled to Bethe-Salpeter equation (BSE) calculations [44–46] become computationally tractable, allowing the determination of both the QP gap and the exciton ground-state energy. The most significant works are mainly devoted to investigate the dielectric screening that affects excitons in TMDCs in the vicinity of graphene- or graphite-thick substrates. In these cases, large band-gap renormalization, on the order of 100 meV, together with a reduction of the exciton binding energy of the same order of magnitude were calculated [20,47]. By using a high-*k* dielectrics environment, such as a Au metal substrate, an even larger band-gap reduction can be achieved for MoS<sub>2</sub> [48] or MoSe<sub>2</sub> MLs [11]. For a MoS<sub>2</sub> ML on a hBN monolayer a band-gap reduction of 40 meV (compared to a freestanding ML) has been reported when a simplified model of bulk hBN is used [49], whereas previous calculations with bulk hBN substrates predicted a 160-meV reduction [50]. A small redshift of the neutral exciton peak (usually denoted *A:1s*), around 20 meV, has also been reported [50] without studying hBN thickness effects. By increasing the capping layer thickness, the change in band gap is expected to occur on an ultrashort length scale since the main contributions to the self-energy are the nonlocal interorbital exchange terms, which directly control the hybridization and the resulting electronic band gap. Since those nonlocal contributions are mainly localized within a radius of about three unit cells [38], we can expect to mimic thick substrate and encapsulation effects by using just a few hBN layers. However, a systematic calculation of the band structure and exciton properties of a TMDC monolayer as a function of the hBN surrounding layer thickness is still lacking. The knowledge of this dependence is crucial for the engineering of vdWHs.

In this paper we have calculated the dependence of both the free-carrier gap  $E_g$  and the binding energy  $E_b$  of the neutral exciton ground state as a function of the hBN layer thickness. As shown in Fig. 1, we demonstrate, thanks to the *GW* + BSE approach that both  $E_g$  and  $E_b$  are efficiently tuned by using an insulating hBN encapsulation layer due to environmental dielectric screening. For thick hBN (>10 MLs), we find a decrease in the exciton binding energy by about 27%, i.e., 160 meV (compared to freestanding ML) as extrapolated in

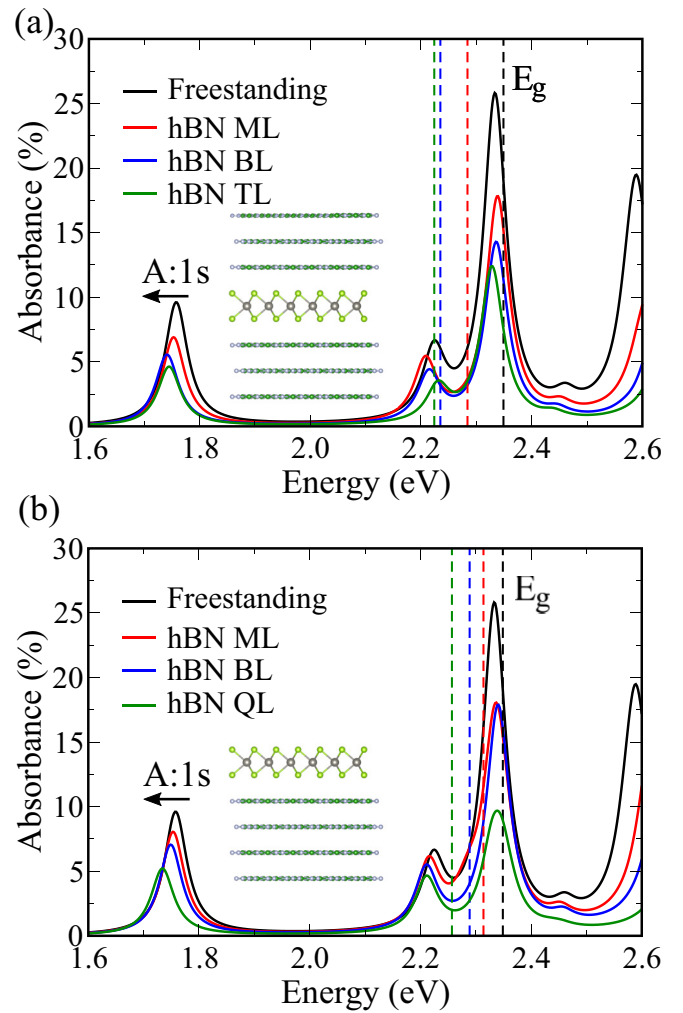


FIG. 1. (a) Absorbance spectra of a WSe<sub>2</sub> monolayer encapsulated by hBN monolayers, bilayers (BLs), or trilayers (TLs). (b) Absorbance spectra of a WSe<sub>2</sub> monolayer stacked on hBN mono-, bi-, or quadrilayers (QLs). The corresponding fundamental band-gap ( $E_g$ ) values are given by dashed lines when the insets recall the stacking geometries: W and Se are in gray and light green, respectively, when B and N are in light blue and green.

Fig. 2. These results are in rather good agreement with recent measurements [10,19,22,51]. The striking feature is that the encapsulation of the WSe<sub>2</sub> monolayer by only three sheets of hBN ( $\sim 1$  nm) already yields a 20% reduction of the exciton binding energy. As expected, a lower binding energy reduction occurs when hBN is only used as a substrate. We also show that the QEH model tends to overestimate the reduction of the binding energies when compared to our first-principles calculations in both stacking configurations.

## COMPUTATIONAL DETAILS

The atomic structures, the quasiparticle band structures, and optical spectra are obtained from DFT calculations using the VASP package [52,53]. It uses the plane-augmented-wave scheme [54,55] to treat core electrons. Three, five, six, and 14 electrons have been explicitly included in the valence states for B, N, Se, and W, respectively. The

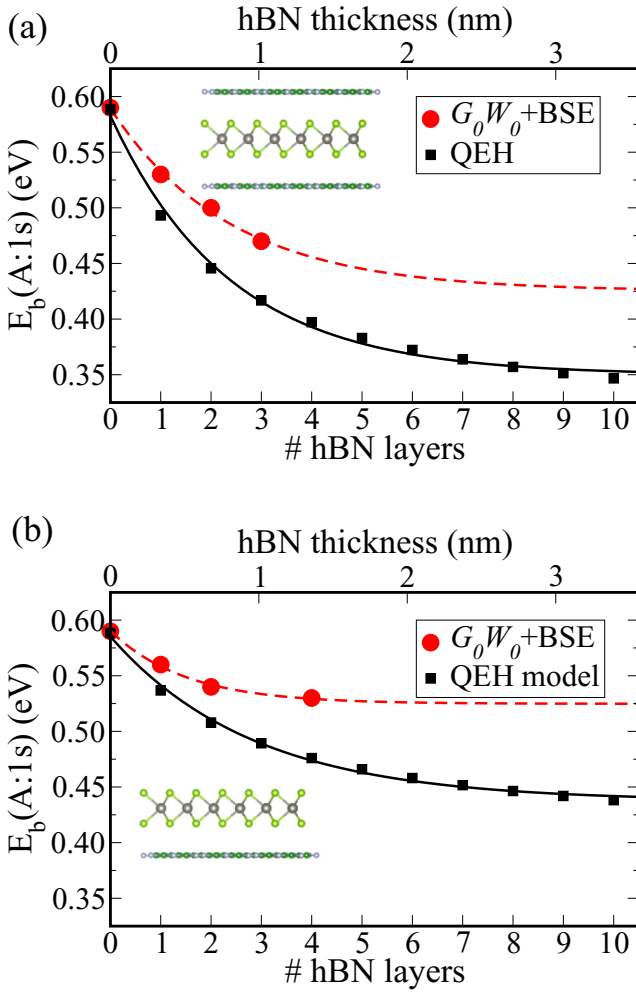


FIG. 2. Evolution of the A:1s exciton binding energy with respect to hBN thickness using the  $G_0W_0$  + BSE and QE models of Ref. [34] (a) when hBN is used for encapsulation and (b) is used as substrate. The bold and dashed lines correspond to interpolated curves using exponential decay curves. The insets recall the stacking geometries: W and Se are in gray and light green, respectively, when B and N are in light blue and green.

Perdew-Burke-Ernzerhof (PBE) functional [56] is used as an approximation of the exchange-correlation electronic term to build the wave function, which serves as a starting point for further  $G_0W_0$  calculations. During the geometry's optimization step of all the heterostructures performed at the PBE-D3 level [57], all the atoms were allowed to relax with a force convergence criterion below  $0.005 \text{ eV/\AA}$  in order to include the van der Waals interaction between layers. The optimized lattice parameter of  $\text{WSe}_2$  used for all calculations is  $3.32 \text{ \AA}$ . The coincidence lattice method for 2D crystals as proposed in Ref. [43] has been used to generate computationally tractable supercells, with the aim of also minimizing the strain on hBN layers. Thanks to the CELLMATCH software [58], we have generated the hBN/ $\text{WSe}_2$  supercell with the following parameter: a  $(\sqrt{7} \times \sqrt{7})R19.1^\circ/(2 \times 2)$  as shown in Fig. 3, which corresponds to biaxial strain of 0.5% on the hBN layers. Within this geometry two stacking orderings are available: either the Se atom in the  $(1/3, 1/3)$  position is lying above

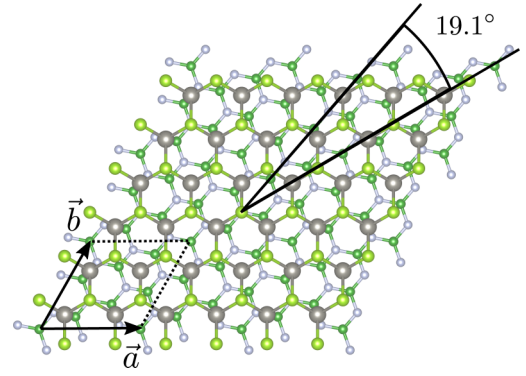


FIG. 3. Schematic of the hBN/ $\text{WSe}_2$  lattice structure presenting the calculation cell  $(\vec{a}, \vec{b})$  with a  $19.1^\circ$  rotation between both lattices, W and Se are in gray and light green, respectively, when B and N are in light blue and green.

a B or a N atom. In the case of a single hBN ML, the energy difference between the two stackings is less than 1 meV when the interlayer distances ( $d$ ) are 3.42 and 3.48  $\text{\AA}$  for B aligned and N aligned, respectively. When including more hBN layers, we have used  $AA'$ -stacked geometry yielding a hBN-hBN interlayer distance of 3.39  $\text{\AA}$  since it appears that the eclipsed configuration is the most stable one for hBN bulk and bilayers [59]. Effective band structures on top of PBE calculations have been calculated using the unfolding techniques proposed in Refs. [60,61].

A grid of  $6 \times 6 \times 1$   $k$  points has been used in conjunction with a vacuum height of 18.4  $\text{\AA}$  for all calculation cells to benefit from the error's cancellation in the band-gap estimates [62] and to provide absorption spectra in good agreement with experiments [63,64]. An energy cutoff of 400 eV and a Gaussian smearing of 0.05-eV width have been chosen for partial occupancies when a tight electronic minimization tolerance of  $10^{-8}$  eV is set to determine with good precision the corresponding derivative of the orbitals with respect to  $k$  needed in quasiparticle band-structure calculations. Spin-orbit coupling (SOC) was also included non-self-consistently to determine eigenvalues and wave functions as input for the full-frequency-dependent  $GW$  calculations [65] performed at the  $G_0W_0$  level [66]. The total number of states included in the  $GW$  procedure is set to 960, in conjunction with an energy cutoff of 100 eV for the response function, after a careful check of the direct band-gap convergence (smaller than 0.1 eV as a function of  $k$ -point sampling). All optical excitonic transitions have been calculated by solving the Bethe-Salpeter equation as follows [45,46]:

$$(\varepsilon_c^{\text{QP}} - \varepsilon_v^{\text{QP}})A_{vc} + \sum_{v'c'} \langle v c | K^{eh} | v' c' \rangle A_{v'c'} = \Omega A_{vc}, \quad (1)$$

where  $\Omega$ 's are the resulting  $e$ - $h$  excitation energies.  $A_{vc}$ 's are the corresponding eigenvectors when  $\varepsilon^{QP}$  are the single-quasi-particle energies obtained at the  $G_0W_0$  level, and  $K^{eh}$  is the conduction band electron - valence band hole interaction kernel. This term consists of a first attractive screened direct term and a repulsive exchange part. Practically we have included the eight highest valence bands and the 12 lowest conduction bands to obtain eigenvalues and oscillator

TABLE I. Calculated WSe<sub>2</sub> monolayer quasiparticle band gaps from DFT and  $G_0W_0$  and  $A$  and  $B$  exciton peak positions in eV upon encapsulation with hBN layers (upper part of the table) or substrate modeling.

	DFT	$G_0W_0$	$A$	$B$
Freestanding	1.28	2.35	1.76	2.22
hBN ML encapsulation	1.25	2.28	1.75	2.21
hBN BL encapsulation	1.25	2.24	1.74	2.21
hBN TL encapsulation	1.25	2.22	1.75	2.23
hBN ML substrate	1.25	2.30	1.74	2.20
hBN BL substrate	1.25	2.29	1.75	2.21
hBN QL substrate	1.25	2.26	1.73	2.21

strengths on all systems. From these calculations, we report the absorbance values by using the imaginary part of the complex dielectric function  $\epsilon_2(\omega)$  with the following formula [67]:

$$A(\omega) = \frac{\omega}{c} \epsilon_2(\omega) \Delta z, \quad (2)$$

where  $\Delta z$  is the vacuum distance between periodic images thus this quantity should not depend on the size of calculation cells in the perpendicular direction. As pointed out by Bernardi *et al.* [68], Eq. (2) is a Taylor expansion for  $\Delta z \rightarrow 0$  of the absorbance defined as  $A = 1 - e^{-\alpha_2 \Delta z}$  for a single or bilayer of a bulk material with a thickness  $\Delta z$ , presenting an absorption coefficient of  $\alpha_2(\omega) = \frac{\omega \epsilon_2(\omega)}{cn(\omega)}$ ; here the refractive index is  $n = 1$  since the considered heterostructure is surrounded by vacuum only. The computational setup used to extract the binding energies out of the QEH model in Fig. 2 is the following: The hBN-hBN and WSe<sub>2</sub>-hBN distances are 3.4 and 4.7 Å, respectively, as in DFT calculations. An effective mass of  $0.29m_0$  is used to yield the same binding energy of the  $A:1s$  exciton as in our  $G_0W_0 + \text{BSE}$  calculations.

#### BAND-GAP VARIATIONS WITH THE DIELECTRIC ENVIRONMENT

Absorption spectra of an encapsulated WSe<sub>2</sub> ML with three different hBN thicknesses, ML, BLs, and TLs are presented and compared to the ideal freestanding configuration in Fig. 1(a). Our  $GW$  calculations performed on the freestanding ML exhibit a direct QP band gap at the  $K$  point with a value of 2.35 eV and a ground-state exciton energy (“optical gap”) of 1.76 eV. Consequently, the binding energy of the lowest-energy exciton ( $A:1s$ ) is 0.59 eV. These two values are in line with previous theoretical and recent experimental studies [8,10,66,69]. Table I summarizes QP (calculated at the  $G_0W_0$  level) and DFT band gaps as well as  $A$  and  $B$  ground-state exciton peak positions for different dielectric environments. If the surrounding dielectric environment screens efficiently the electron-hole interaction by decreasing the  $A$  peak positions and at the same time reduces the fundamental band gap, it also leaves the  $A$ - $B$  splitting unchanged. This confirms that this splitting is solely due to SOC and it remains largely unaffected by the presence of any dielectric environment.

Upon encapsulation we observe a decrease in the QP band gap by already 110 meV when hBN BLs are used when it

becomes 130 meV for TLs [Fig. 1(a)], i.e., a decrease of 6%. This means that the very thin hBN environment has a significant effect on the screening of the interactions within the TMDC sheet. We have also investigated the energy changes if hBN lies only on one side of the TMDC ML [Fig. 1(b)]. When the WSe<sub>2</sub> is stacked on a hBN QL the corresponding QP band gap is also significantly reduced by 90 meV. This value is in good agreement with the recent measurement of the QP band-gap change ( $\sim 100$  meV) between a WSe<sub>2</sub> ML deposited on an 8-nm hBN layer and a WSe<sub>2</sub> ML deposited on a thick SiO<sub>2</sub> [19]. Moreover in Ref. [49], a value of a 40-meV QP energy change was reported in the case of a MoS<sub>2</sub> ML on hBN, whereas it is extrapolated to be 160 meV in the work of Drüppel *et al.* [50]. It can be even larger depending on the approaches: Band-gap reductions of 15% and 13% can be extracted from Refs. [32,33], for instance. Those results stress the importance of using post-DFT approaches that account for many-body term corrections to the self-energy of electrons in such vdWH structures. Indeed, Table I shows that the band-gap reduction is much smaller (30 meV) for the same systems at the PBE level of theory and there is no distinction between the stacking or the encapsulation situations. More importantly, the independent particle band-gap value already saturates even in the case of the TMDC ML in an interaction with a single hBN layer, see Table I.

The limitation of standard DFT to investigate electronic properties of vdWHs is also clearly shown in Fig. 4 where no differences in the effective band structure of hBN BL/WSe<sub>2</sub>/hBN BL and hBN QL/WSe<sub>2</sub>/hBN QL stackings are visible. Interestingly when comparing with the effective band structure of a freestanding ML, the presence of the surrounding hBN layers’ environment always pushes upward the valence-band maxima in  $\Gamma$  as well as in the conduction-band minima in the valley ( $Q$ ) located between  $K$  and  $\Gamma$  points. The origins of the too small band-gap values and the limited effects due to the presence of hBN layers for this level of calculation are as follows: (i) the lack of self-energy correction in a standard PBE type of calculations and (ii) the exponential decay of the exchange term, which is essentially based on a Slater-Dirac expression which roughly behaves as  $\rho^{4/3}$  where  $\rho$  stands for the electronic density despite gradient corrections [70]. As a consequence, at the standard DFT level, the presence of hBN layers does not significantly change the calculated band-gap value since the dielectric environment does not affect the TMDC intralayer hybridization between the  $d$  orbitals of the TM and the  $p$  orbitals of the chalcogens, which controls the gap opening in the  $K$  valley between the  $d_{z^2}$  and the  $d_{xy}$ ,  $d_{x^2-y^2}$  states [71]. This limitation of standard DFT calculations has been recently reported in the same context of varying the dielectric environment of TMDC MLs [49].

#### EXCITON ENERGY VARIATIONS WITH THE DIELECTRIC ENVIRONMENT

Additionally, for the reduction of the band gap, one can observe in Fig. 1(a) a slight redshift of the  $A:1s$  exciton peak when the hBN encapsulation layer thickness increases. Upon a hBN TL encapsulation, the calculated shift towards lower energy is around 20 meV, compared to the

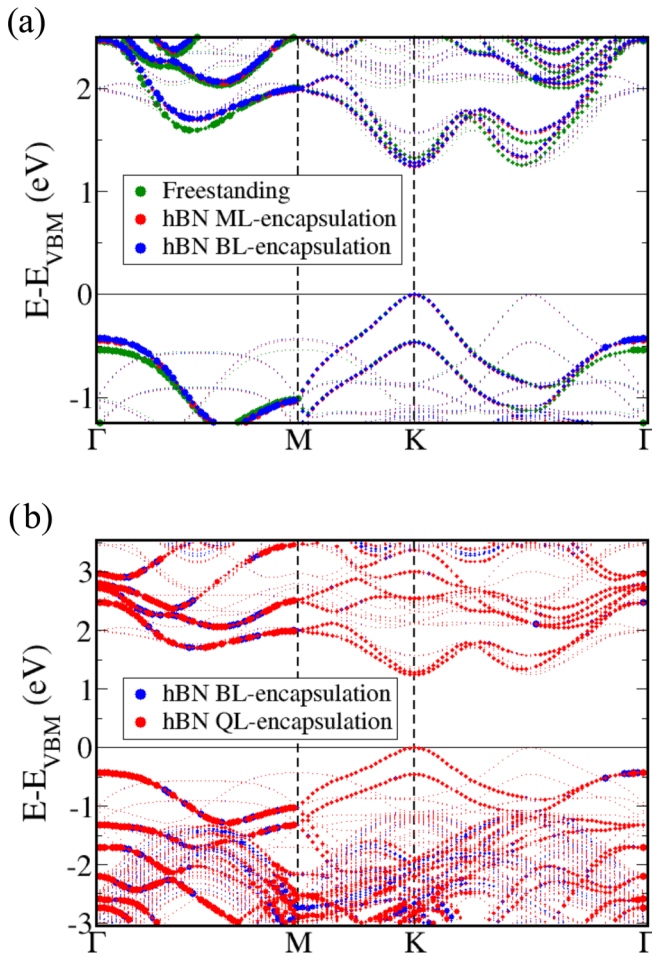


FIG. 4. (a) Evolution of the effective band structure at the PBE level upon encapsulation with hBN layers of a WSe<sub>2</sub> ML with 1 ML of hBN (red) on each side or 1 BL of hBN on each side (blue). Mind that the BL and ML encapsulation situations are almost superimposed over the entire first-Brillouin zone. (b) Comparison of the effective band structure of a WSe<sub>2</sub> ML encapsulated by hBN BLs and hBN QLs, showing that the PBE level of calculations misses long-range electronic screening since the two band structures are superimposed over the entire first-Brillouin zone.

freestanding ML. With a hBN QL serving as a substrate model, we obtain a redshift of roughly 30 meV, Fig. 1(b). As expected these shifts remain much smaller compared to the band-gap renormalization due to the simultaneous reduction of the exciton binding energies of the *A*:1s exciton. Our calculated reduction of exciton energies is in agreement with recent measurements [10,19,22]. For instance, Borghardt *et al.* [10] reported redshifts of the neutral exciton emission energies from  $\mu$ -photoluminescence experiments when hBN was used as a substrate (17 meV) or for encapsulation (35 meV). This trend was also evidenced in a recent theoretical work on excitons and trions in MoS<sub>2</sub> MLs on different substrates [50] or encapsulated [32]. When a MoS<sub>2</sub> ML is encapsulated, the theoretical redshift of the *A* peak is 50 meV. It also agrees with the results obtained by a static Coulomb-hole plus a screened exchange tight-binding approach [33].

All together, our calculations displayed in Fig. 2 show that the fundamental excitonic binding energy reduction using

three hBN layers (TL) is 120 meV compared to a free-standing ML. We have used a simple exponential decay law to extrapolate the *A*:1s exciton binding energies from the  $G_0W_0 + \text{BSE}$  and QEH data. After stacking ten hBN layers ( $\sim 3$  nm), the binding energy becomes clearly insensitive to the use of additional layers. The maximal reduction of the binding energy of the *A*:1s exciton is then around 27% upon hBN encapsulation. This calculated binding energy reduction is in line with the experimental determination of the effect of the surrounding dielectric environment, Refs. [10,17,51]. Moreover, we note in Fig. 1 a clear decrease in the exciton absorbance upon encapsulation. This is perfectly consistent with the decrease in the exciton oscillator strength resulting from the reduction of its binding energy. We have compared our results to the ones obtained with the QEH model. It consists of a semiclassical approach which takes as input the static dielectric functions of the individual isolated layers at the random-phase approximation (RPA) level of theory on top of local density approximation Kohn-Sham orbitals and couples them classically via their long-range Coulomb interaction [41]. In order to get the exciton properties, this method, which yields the global vdWH dielectric function, is combined in a second time to a generalized 2D Mott-Wannier exciton model.

Figure 2 compares the variation of the ground-state exciton binding energy with our fully *ab initio* approach and the QEH model using hBN encapsulation and hBN as a substrate. When the hBN thickness increases, similar trends are observed with both calculation methods. However, for thick hBN thickness (approximately ten monolayers, i.e., 3 nm), the reduction is much larger, around 40%, for the QEH model, compared to our calculations ( $\sim 27\%$ ). One can suspect that, as proposed in Ref. [12], the too strong screening in the QEH model originates from the absence of interlayer gaps in the vdWH building. Another possibility could be that static dielectric constants at the RPA level on top of DFT orbitals are usually overestimated by 5–20% or even more depending on the bulk materials' nature [72]. Moreover, as stressed by Stier *et al.*, the use of high-frequency dielectric constants instead of the static ones appears more founded since a dielectric material should respond to an exciton formation at a characteristic frequency closed to its binding energy values [51]. To the best of our knowledge no experimental data on the variation of the exciton binding energy of a WSe<sub>2</sub> ML as a function of the hBN thickness are available. Nevertheless, in a quite similar situation, the measured variation of the exciton energy of a WS<sub>2</sub> ML as a function of the number of graphene capping layers also shows that: (i) The QEH model overestimates the redshift [19], and (ii) similar to our calculation, the effects of screening is very short ranged: Even a single graphene layer already has a very significant impact on the exciton binding energy.

## CONCLUSION

We have calculated the dependence of both the quasiparticle band-gap  $E_g$  and the binding energy  $E_b$  of the neutral exciton ground state in a WSe<sub>2</sub> monolayer as a function of the hBN encapsulation layer thickness. Our approach consists of solving the Bethe-Salpeter equation on top of *GW*

wave functions built from standard DFT calculations. Our calculations show the large variation of both  $E_g$  and  $E_b$  as a consequence of the tuning of the monolayer surrounding the dielectric environment. The key result is that the encapsulation of the WSe<sub>2</sub> monolayer by only three sheets of hBN ( $\sim 1$  nm) already yields a 20% reduction of the exciton binding energy, whereas the maximal reduction for a thick hBN layer is  $\sim 27\%$ . As expected, a smaller binding energy reduction occurs when hBN is only used as a substrate. We also show that the quantum electrostatic heterostructure model tends to overestimate the reduction of the binding energies when compared to our first-principles calculations in both stacking configurations. These results can be very useful to engineer the exciton properties in new van der Waals heterostructures.

Unfortunately, our computational setup does not allow the determination of the effect of dielectric screening on the excited states of the excitons; this point certainly deserves further work in relation with recent experimental work [10,18,25,51].

#### ACKNOWLEDGMENTS

I. C. Gerber thanks the CALMIP initiative for the generous allocation of computational time through Project No. p0812 as well as the GENCI-CINES and GENCI-IDRIS for Grant No. A004096649. X. Marie acknowledges the Institut Universitaire de France and the ANR MagicValley Project (ANR-18-CE24-0007-03).

- 
- [1] G. Wang, A. Chernikov, M. M. Glazov, T. F. Heinz, X. Marie, T. Amand, and B. Urbaszek, *Rev. Mod. Phys.* **90**, 021001 (2018).
- [2] K. F. Mak, C. Lee, J. Hone, J. Shan, and T. F. Heinz, *Phys. Rev. Lett.* **105**, 136805 (2010).
- [3] A. Splendiani, L. Sun, Y. Zhang, T. Li, J. Kim, C.-Y. Chim, G. Galli, and F. Wang, *Nano Lett.* **10**, 1271 (2010).
- [4] Q. H. Wang, K. Kalantar-Zadeh, A. Kis, J. N. Coleman, and M. S. Strano, *Nat. Nanotechnol.* **7**, 699 (2012).
- [5] A. Chernikov, T. C. Berkelbach, H. M. Hill, A. Rigosi, Y. Li, O. B. Aslan, D. R. Reichman, M. S. Hybertsen, and T. F. Heinz, *Phys. Rev. Lett.* **113**, 076802 (2014).
- [6] Z. Ye, T. Cao, K. O'Brien, H. Zhu, X. Yin, Y. Wang, S. G. Louie, and X. Zhang, *Nature (London)* **513**, 214 (2014).
- [7] K. He, N. Kumar, L. Zhao, Z. Wang, K. F. Mak, H. Zhao, and J. Shan, *Phys. Rev. Lett.* **113**, 026803 (2014).
- [8] G. Wang, X. Marie, I. Gerber, T. Amand, D. Lagarde, L. Bouet, M. Vidal, A. Balocchi, and B. Urbaszek, *Phys. Rev. Lett.* **114**, 097403 (2015).
- [9] Y. Lin, X. Ling, L. Yu, S. Huang, A. L. Hsu, Y.-H. Lee, J. Kong, M. S. Dresselhaus, and T. Palacios, *Nano Lett.* **14**, 5569 (2014).
- [10] S. Borghardt, J.-S. Tu, F. Winkler, J. Schubert, W. Zander, K. Leosson, and B. E. Kardynał, *Phys. Rev. Mater.* **1**, 054001 (2017).
- [11] G. Gupta, S. Kallatt, and K. Majumdar, *Phys. Rev. B* **96**, 081403(R) (2017).
- [12] M. Florian, M. Hartmann, A. Steinhoff, J. Klein, A. W. Holleitner, J. J. Finley, T. O. Wehling, M. Kaniber, and C. Gies, *Nano Lett.* **18**, 2725 (2018).
- [13] S. Park, N. Mutz, T. Schultz, S. Blumstengel, A. Han, A. Aljarb, L.-J. Li, E. J. W. List-Kratochvil, P. Amsalem, and N. Koch, *2D Mater.* **5**, 025003 (2018).
- [14] D. Vaclavkova, J. Wyzula, K. Nogajewski, M. Bartos, A. O. Slobodeniuk, C. Faugeras, M. Potemski, and M. R. Molas, *Nanotechnology* **29**, 325705 (2018).
- [15] Z. Hu, Z. Wu, C. Han, J. He, Z. Ni, and W. Chen, *Chem. Soc. Rev.* **47**, 3100 (2018).
- [16] M. Van der Donck and F. M. Peeters, *Phys. Rev. B* **98**, 115104 (2018).
- [17] A. V. Stier, N. P. Wilson, G. Clark, X. Xu, and S. A. Crooker, *Nano Lett.* **16**, 7054 (2016).
- [18] J. Zipfel, J. Holler, A. A. Mitoglu, M. V. Ballottin, P. Nagler, A. V. Stier, T. Taniguchi, K. Watanabe, S. A. Crooker, P. C. M. Christianen *et al.*, *Phys. Rev. B* **98**, 075438 (2018).
- [19] A. Raja, A. Chaves, J. Yu, G. Arefe, H. M. Hill, A. F. Rigosi, T. C. Berkelbach, P. Nagler, C. Schüller, T. Korn *et al.*, *Nat. Commun.* **8**, 15251 (2017).
- [20] M. M. Ugeda, A. J. Bradley, S.-F. Shi, F. H. da Jornada, Y. Zhang, D. Y. Qiu, W. Ruan, S.-K. Mo, Z. Hussain, Z.-X. Shen *et al.*, *Nature Mater.* **13**, 1091 (2014).
- [21] Y. Wang, S. Zhang, D. Huang, J. Cheng, Y. Li, and S. Wu, *2D Mater.* **4**, 015021 (2017).
- [22] F. Cadiz, E. Courtade, C. Robert, G. Wang, Y. Shen, H. Cai, T. Taniguchi, K. Watanabe, H. Carrere, D. Lagarde *et al.*, *Phys. Rev. X* **7**, 021026 (2017).
- [23] M. Manca, C. Robert, F. Cadiz, T. Taniguchi, K. Watanabe, E. Courtade, T. Amand, P. Renucci, X. Marie, M. M. Glazov *et al.*, *Nat. Commun.* **8**, 14927 (2017).
- [24] O. A. Ajayi, J. V. Ardelean, G. D. Shepard, J. Wang, A. Antony, T. Taniguchi, K. Watanabe, T. F. Heinz, S. Strauf, X. Y. Zhu *et al.*, *2D Mater.* **4**, 031011 (2017).
- [25] C. Robert, M. A. Semina, F. Cadiz, M. Manca, E. Courtade, T. Taniguchi, K. Watanabe, H. Cai, S. Tongay, B. Lassagne *et al.*, *Phys. Rev. Mater.* **2**, 011001 (2018).
- [26] G. Scuri, Y. Zhou, A. A. High, D. S. Wild, C. Shu, K. De Greve, L. A. Jauregui, T. Taniguchi, K. Watanabe, P. Kim *et al.*, *Phys. Rev. Lett.* **120**, 037402 (2018).
- [27] P. Back, S. Zeytinoglu, A. Ijaz, M. Kroner, and A. Imamoğlu, *Phys. Rev. Lett.* **120**, 037401 (2018).
- [28] N. S. Rytova, *Proc. MSU, Phys. Astron.* **3**, 30 (1967).
- [29] L. V. Keldysh, *JETP Lett.* **29**, 658 (1979).
- [30] P. Cudazzo, I. V. Tokatly, and A. Rubio, *Phys. Rev. B* **84**, 085406 (2011).
- [31] D. Van Tuan, M. Yang, and H. Dery, *Phys. Rev. B* **98**, 125308 (2018).
- [32] L. Meckbach, T. Stroucken, and S. W. Koch, *Phys. Rev. B* **97**, 035425 (2018).
- [33] Y. Cho and T. C. Berkelbach, *Phys. Rev. B* **97**, 041409(R) (2018).
- [34] S. Latini, T. Olsen, and K. S. Thygesen, *Phys. Rev. B* **92**, 245123 (2015).
- [35] I. Kylänpää and H.-P. Komsa, *Phys. Rev. B* **92**, 205418 (2015).

- [36] M. L. Trolle, T. G. Pedersen, and V. Véniard, *Sci. Rep.* **7**, 39844 (2017).
- [37] A. Steinhoff, T. O. Wehling, and M. Rösner, *Phys. Rev. B* **98**, 045304 (2018).
- [38] M. Rösner, C. Steinke, M. Lorke, C. Gies, F. Jahnke, and T. O. Wehling, *Nano Lett.* **16**, 2322 (2016).
- [39] A. R. Klots, B. Weintrub, D. Prasai, D. Kidd, K. Varga, K. A. Velizhanin, and K. I. Bolotin, *Sci. Rep.* **8**, 768 (2018).
- [40] L. S. R. Cavalcante, A. Chaves, B. Van Duppen, F. M. Peeters, and D. R. Reichman, *Phys. Rev. B* **97**, 125427 (2018).
- [41] K. Andersen, S. Latini, and K. S. Thygesen, *Nano Lett.* **15**, 4616 (2015).
- [42] S. Latini, K. T. Winther, T. Olsen, and K. S. Thygesen, *Nano Lett.* **17**, 938 (2017).
- [43] D. S. Koda, F. Bechstedt, M. Marques, and L. K. Teles, *J. Phys. Chem. C* **120**, 10895 (2016).
- [44] L. Hedin, *Phys. Rev.* **139**, A796 (1965).
- [45] W. Hanke and L. J. Sham, *Phys. Rev. Lett.* **43**, 387 (1979).
- [46] M. Rohlfling and S. G. Louie, *Phys. Rev. Lett.* **81**, 2312 (1998).
- [47] K. T. Winther and K. S. Thygesen, *2D Mater.* **4**, 025059 (2017).
- [48] J. Ryou, Y.-S. Kim, S. KC, and K. Cho, *Sci. Rep.* **6**, 291848 (2016).
- [49] M. H. Naik and M. Jain, *Phys. Rev. Mater.* **2**, 084002 (2018).
- [50] M. Drüppel, T. Deilmann, P. Krüger, and M. Rohlfling, *Nat. Commun.* **8**, 2117 (2017).
- [51] A. V. Stier, N. P. Wilson, K. A. Velizhanin, J. Kono, X. Xu, and S. A. Crooker, *Phys. Rev. Lett.* **120**, 057405 (2018).
- [52] G. Kresse and J. Hafner, *Phys. Rev. B* **47**, 558 (1993).
- [53] G. Kresse and J. Furthmüller, *Phys. Rev. B* **54**, 11169 (1996).
- [54] P. E. Blöchl, *Phys. Rev. B* **50**, 17953 (1994).
- [55] G. Kresse and D. Joubert, *Phys. Rev. B* **59**, 1758 (1999).
- [56] J. P. Perdew, K. Burke, and M. Ernzerhof, *Phys. Rev. Lett.* **77**, 3865 (1996).
- [57] S. Grimme, J. Antony, S. Ehrlich, and H. Krieg, *J. Chem. Phys.* **132**, 154104 (2010).
- [58] P. Lazić, *Comput. Phys. Commun.* **197**, 324 (2015).
- [59] G. Constantinescu, A. Kuc, and T. Heine, *Phys. Rev. Lett.* **111**, 036104 (2013).
- [60] P. V. C. Medeiros, S. Stafström, and J. Björk, *Phys. Rev. B* **89**, 041407 (2014).
- [61] P. V. C. Medeiros, S. S. Tsirkin, S. Stafström, and J. Björk, *Phys. Rev. B* **91**, 041116 (2015).
- [62] F. Hüser, T. Olsen, and K. S. Thygesen, *Phys. Rev. B* **88**, 245309 (2013).
- [63] A. R. Klots, A. K. M. Newaz, B. Wang, D. Prasai, H. Krzyzanowska, J. Lin, D. Caudel, N. J. Ghimire, J. Yan, B. L. Ivanov *et al.*, *Sci. Rep.* **4**, 6608 (2014).
- [64] A. Molina-Sánchez, D. Sangalli, K. Hummer, A. Marini, and L. Wirtz, *Phys. Rev. B* **88**, 045412 (2013).
- [65] M. Shishkin and G. Kresse, *Phys. Rev. B* **74**, 035101 (2006).
- [66] J. P. Echeverry, B. Urbaszek, T. Amand, X. Marie, and I. C. Gerber, *Phys. Rev. B* **93**, 121107(R) (2016).
- [67] L. Yang, J. Deslippe, C.-H. Park, M. L. Cohen, and S. G. Louie, *Phys. Rev. Lett.* **103**, 186802 (2009).
- [68] M. Bernardi, M. Palummo, and J. C. Grossman, *Nano Lett.* **13**, 3664 (2013).
- [69] A. Ramasubramaniam, *Phys. Rev. B* **86**, 115409 (2012).
- [70] A. D. Becke, *Phys. Rev. A* **38**, 3098 (1988).
- [71] L. F. Mattheiss, *Phys. Rev. B* **8**, 3719 (1973).
- [72] M. Gajdoš, K. Hummer, G. Kresse, J. Furthmüller, and F. Bechstedt, *Phys. Rev. B* **73**, 045112 (2006).